AFRL-RX-WP-TP-2009-4198

COARSE-GRAINED MOLECULAR DYNAMICS SIMULATION OF IONIC POLYMER NETWORKS (Postprint)

T.E. Dirama, V. Varshney, K.L. Anderson, J.A. Shumaker, and J.A. Johnson

Nonmetallic Materials Division
Materials and Manufacturing Directorate

JULY 2008
Interim Report

Approved for public release; distribution unlimited.

See additional restrictions described on inside pages

STINFO COPY

©2008 Springer Science+Business Media, B.V.

AIR FORCE RESEARCH LABORATORY
MATERIALS AND MANUFACTURING DIRECTORATE
WRIGHT-PATTERSON AIR FORCE BASE, OH 45433-7750
AIR FORCE MATERIEL COMMAND
UNITED STATES AIR FORCE

NOTICE AND SIGNATURE PAGE

Using Government drawings, specifications, or other data included in this document for any purpose other than Government procurement does not in any way obligate the U.S. Government. The fact that the Government formulated or supplied the drawings, specifications, or other data does not license the holder or any other person or corporation; or convey any rights or permission to manufacture, use, or sell any patented invention that may relate to them.

This report was cleared for public release by the Wright-Patterson Air Force Base (WPAFB) Public Affairs Office and is available to the general public, including foreign nationals. Copies may be obtained from the Defense Technical Information Center (DTIC) (http://www.dtic.mil).

AFRL-RX-WP-TP-2009-4198 HAS BEEN REVIEWED AND IS APPROVED FOR PUBLICATION IN ACCORDANCE WITH THE ASSIGNED DISTRIBUTION STATEMENT.

//signature//	//signature//
LT MEGAN LEGENDRE Program Manager Coatings Technology Integration Logistics Systems Support Branch	DANIEL J. McDERMOTT Deputy Chief System Support Division Materials & Manufacturing Directorate

This report is published in the interest of scientific and technical information exchange, and its publication does not constitute the Government's approval or disapproval of its ideas or findings.

*Disseminated copies will show "//signature//" stamped or typed above the signature blocks.

REPORT DOCUMENTATION PAGE

Form Approved
OMB No. 0704-0188

The public reporting burden for this collection of information is estimated to average 1 hour per response, including the time for reviewing instructions, searching existing data sources, searching existing data sources, gathering and maintaining the data needed, and completing and reviewing the collection of information. Send comments regarding this burden estimate or any other aspect of this collection of information, including suggestions for reducing this burden, to Department of Defense, Washington Headquarters Services, Directorate for Information Operations and Reports (0704-0188), 1215 Jefferson Davis Highway, Suite 1204, Arlington, VA 22202-4302. Respondents should be aware that notwithstanding any other provision of law, no person shall be subject to any penalty for failing to comply with a collection of information if it does not display a currently valid OMB control number. **PLEASE DO NOT RETURN YOUR FORM TO THE ABOVE ADDRESS**.

1. REPORT DATE *(DD-MM-YY)*	2. REPORT TYPE	3. DATES COVERED *(From - To)*
July 2008	Journal Article Postprint	08 June 2006 – 25 January 2008

4. TITLE AND SUBTITLE
COARSE-GRAINED MOLECULAR DYNAMICS SIMULATION OF IONIC POLYMER NETWORKS (Postprint)

5a. CONTRACT NUMBER
FA8650-05-D-5807-0052

5b. GRANT NUMBER

5c. PROGRAM ELEMENT NUMBER
62102F

6. AUTHOR(S)
T.E. Dirama and V. Varshney (Universal Technology Corporation)
K.L. Anderson (Procter & Gamble)
J.A. Shumaker (University of Dayton Research Institute)
J.A. Johnson (Materials and Manufacturing Directorate, Nonmetallic Materials Division (AFRL/RXB))

5d. PROJECT NUMBER
4347

5e. TASK NUMBER
RG

5f. WORK UNIT NUMBER
M06R3000

7. PERFORMING ORGANIZATION NAME(S) AND ADDRESS(ES)

Nonmetallic Materials Division (AFRL/RXB)
Materials and Manufacturing Directorate
Wright-Patterson Air Force Base, OH 45433-7750
Air Force Materiel Command
United States Air Force

Universal Technology Corporation
Procter & Gamble
University of Dayton Research Institute

8. PERFORMING ORGANIZATION REPORT NUMBER
DOI 10.1007/s11043-008-9058-5

9. SPONSORING/MONITORING AGENCY NAME(S) AND ADDRESS(ES)

Air Force Research Laboratory
Materials and Manufacturing Directorate
Wright-Patterson Air Force Base, OH 45433-7750
Air Force Materiel Command
United States Air Force

10. SPONSORING/MONITORING AGENCY ACRONYM(S)
AFRL/RXSS

11. SPONSORING/MONITORING AGENCY REPORT NUMBER(S)
AFRL-RX-WP-TP-2009-4198

12. DISTRIBUTION/AVAILABILITY STATEMENT
Approved for public release; distribution unlimited.

13. SUPPLEMENTARY NOTES
PAO case number WPAFB 09-0841; date cleared: 09 April 2009. ©2008 Springer Science+Business Media, B.V. The U.S. Government is joint author of the work and has the right to use, modify, reproduce, release, perform, display, or disclose the work. Published in Mech Time-Depend Mater (2008) 12:205-220.

14. ABSTRACT
The stress-strain behavior of cross-linked polymeric networks was investigated using molecular dynamics simulations with a coarse-grained representation of the repeating units. The network structure was formed by dynamically cross-linking the reactants placed between two rigid layers comprised of particles of the same type. We studied two types of networks which differ only by one containing ionic pairs that amount to 7% of the total number of bonds present. The stress-strain curves were obtained after imposing deformation in tensile and shear modes to the networks and measuring their stress response. Under both forms of deformations there was improvement in the level of stress that the material could bear. Moreover, the time dependent behavior of the improvement in mechanical properties signed a self-healing mechanism.

15. SUBJECT TERMS
Polymer networks, Self-healing, Ionic bonds, Toughness, Molecular dynamics simulations

16. SECURITY CLASSIFICATION OF:			17. LIMITATION OF ABSTRACT:	18. NUMBER OF PAGES	19a. NAME OF RESPONSIBLE PERSON (Monitor)
a. REPORT	b. ABSTRACT	c. THIS PAGE			LT Megan Legendre, USAF
Unclassified	Unclassified	Unclassified	SAR	22	19b. TELEPHONE NUMBER *(Include Area Code)* (937) 255-2282

Standard Form 298 (Rev. 8-98)
Prescribed by ANSI Std. Z39-18

Mech Time-Depend Mater (2008) 12: 205–220
DOI 10.1007/s11043-008-9058-5

Coarse-grained molecular dynamics simulations of ionic polymer networks

T.E. Dirama · V. Varshney · K.L. Anderson · J.A. Shumaker · J.A. Johnson

Received: 25 February 2008 / Accepted: 11 June 2008 / Published online: 9 July 2008
© Springer Science+Business Media, B. V. 2008

Abstract The stress-strain behavior of cross-linked polymeric networks was investigated using molecular dynamics simulations with a coarse-grained representation of the repeating units. The network structure was formed by dynamically cross-linking the reactants placed between two rigid layers comprised of particles of the same type. We studied two types of networks which differ only by one containing ionic pairs that amount to 7% of the total number of bonds present. The stress-strain curves were obtained after imposing deformation in tensile and shear modes to the networks and measuring their stress response. Under both forms of deformations there was improvement in the level of stress that the material could bear. Moreover, the time dependent behavior of the improvement in mechanical properties signified a self-healing mechanism.

Keywords Polymer networks · Self-healing · Ionic bonds · Toughness · Molecular dynamics simulations · Coarse-grained modeling

1 Introduction

One of the challenges that material science is facing is to design smart materials that can sense the presence of a defect and actively repair the defected area. Such *self-healing* materi-

T.E. Dirama (✉) · V. Varshney
Engineering Division, Universal Technology Corporation, Dayton, OH 45432, USA
e-mail: taner.dirama.ctr@wpafb.af.mil

K.L. Anderson
Procter&Gamble, Corporate Modeling and Simulation, 11810 E. Miami River Road, Cincinnati, OH 45252, USA

J.A. Shumaker
University of Dayton Research Institute, Dayton, OH 45469, USA

J.A. Johnson
Nonmetallic Materials Division, Materials and Manufacturing Directorate, Air Force Research Laboratory, Wright Patterson Air Force Base, OH 45433, USA

als would significantly extend the lifetime and the usefulness of manufactured items (Balazs 2007) such as polymer matrix composites as replacements of metals, and cross-linked systems as adhesives or coatings.

The approaches addressing the self-healing phenomenon in materials science can be categorized in three classes: *the healing with an embedded liquid, the thermally activated solid phase healing* and *the healing of projectile puncture* (Kessler 2007). The first approach involves embedding capsules containing a reactive healing liquid (e.g., resin) that rupture and release the liquid upon deformation. While it has proven to be successful in repairing the damaged area, it has stability issues that occur during processing and the available liquid payload capacity is often limited for various reasons. The second approach provides an improved performance after every cycle of heating, but there is a requirement of external heat supply that makes the process non-autonomic. The third approach has gained recent interest perhaps because it neither requires an external intervention nor has stability issues. It has been shown that the target film (based on ionomers such as copolymers of ethylene and methacrylic acid) that was penetrated by a projectile with a high speed is healed almost instantly to an airtight condition. Essentially, the penetration of the projectile causes localized heating near the puncture which then closes upon itself to heal. The mechanism behind such a self-healing process after the ballistic penetration involves two transformations. First, the film which has been locally melted due to the heat dissipation re-crystallizes and solidifies. Later, the reordering of the physical cross-links takes place. These physical cross-links, according to Eisenberg–Hird–Moore model (Eisenberg et al. 1990), are primary aggregates that consist of several ion pairs known as *multiplets*. These multiplets bring several chains together bound by ionic interaction creating physical cross-links. Calorimetric studies (Tadano et al. 1989) have shown that the re-crystallization occurs rapidly, while the reformation of the physical cross-links is a rather slow process. As a result, the material fully recovers after the latter process is complete.

Highly cross-linked epoxies or polyurethanes are a class of materials that can particularly benefit from a self-healing mechanism. While they possess a variety of appealing properties, two major shortcomings of the highly cross-linked materials are their brittleness and low elongation, which are due to the limited degree of freedom available to the strands between the cross-linking points. The strands extend to their limits even with a small deformation and cause breaking of covalent bonds. Since the covalent bonds are non-reformable, any damage that is caused by impact or elongation will be permanent and cause formation of micro-cracks. For instance, cyclic mechanical loads result in accumulation of the micro-cracks which then leads to catastrophic failure.

The important question is: would a similar idea to that behind the healing of projectile puncture in the thermoplastic ionomers apply to the thermosets? It is known that the breaking of covalent bonds is responsible for reducing the impact resistance properties. The inherent toughness of the network is accommodated mainly by non-covalent interactions such as the van der Waals and the hydrogen bond interactions. Their effectiveness is due to their capability of breaking and displacing under stress to absorb impact energy. However, under high energy impact conditions such weak interactions may not provide a sufficient level of strength in the material. Therefore, in theory, incorporation of stronger, yet reversible ionic bonds (i.e. two neighboring oppositely charged atoms) into the polymeric matrix could be an alternative and effective approach to improve the impact properties. However, one needs to realize that a similar mechanism explained above for the thermoplastic ionomers is an unlikely means for the highly cross-linked materials. First, there will not be re-crystallization since the low degree of freedom in the material prevents crystallization. Secondly, the formation of multiplets is hindered also due to the cross-linked nature of the polymer.

For the cross-linked systems with embedded ionomers one could envision an alternative mechanism in which the multiplets are replaced by ionic pairs and the extent of repairing action is reduced primarily to the length scale of strands between cross-links. A temporary loss of the ionic interaction caused by the deformation can be restored by the same or another pair of ionic groups. Moreover, the addition of ionic pairs which are stronger than the van der Waals and the hydrogen bond interactions, yet still reversible, could serve to increase the bulk material strength and the toughness. The soundness of this probable mechanism can suitably be studied using molecular modeling. Past molecular simulation studies of ionic polymers focused mainly on their charge transport properties associated with applications such as polyelectrolyte membranes in fuel cells (Din and Michaelides 1998; Elliott et al. 1999; Vishnyakov and Neimark 2000). Accordingly, these modeling studies have primarily concerned with the solubility, the conductivity, and the diffusivity rather than mechanical properties.

Computational modeling of networked polymers has gained limited attention in contrast to their widespread use in many applications. The atomistic models of such systems include epoxy resins that were modeled using a single step cross-linking procedure (Yarovsky and Evans 2002) and poly(dimethylsiloxane) (PDMS) network where a dynamical cross-linking procedure was used (Heine et al. 2004). Besides these atomistic models Stevens and coworkers modeled polymeric networks using a coarse-grained representation with the dynamical cross-linking procedure (Stevens 2001; Tsige et al. 2004; Tsige and Stevens 2004). They investigated the effects of the cross-linker functionality, the network connectivity on the mechanical properties and the influence of bond density on interfacial fracture. Their work has shown that a coarse-grained representation enables simulation of the networked systems at longer time and length scales while capturing the experimentally observed essential mechanical features.

Inspired by the success of using ionic interactions in the healing of projectile puncture, here we seek a parallel means of adding self-healing character to cross-linked polymers. Specifically, we investigate the mechanical properties in a polymer network with ion pairs embedded throughout using a generic coarse-grained representation of the system. The ionic pairs were incorporated in an ideal manner as explained later in detail. We explore the possibility of enhancing the toughness by ionic links and the potential underlying mechanisms using molecular dynamics simulations. We have paid attention also to the effect of the rate of deformation applied to the network.

This article is organized as follows. Section 2 describes the details of the model and the simulation protocol. The stress-strain behaviors of the standard and the ionic networks upon deformations in the tensile and shear modes were presented in Sect. 3. The possible mechanisms behind the results were discussed in Sect. 4. The conclusions of this work are given in Sect. 5 followed by the appropriate acknowledgments.

2 Model and simulation protocol

The cross-linked system was represented using the bead-spring model based on the works of Stevens and coworkers (Stevens 2001; Tsige et al. 2004; Tsige and Stevens 2004). The interactions between the beads were described using 6–12 Lennard-Jones (LJ) potential (see (1)) with a $2.5d$ cutoff

$$U_{\mathrm{LJ}}(r) = 4u_0\left[\left(\frac{d}{r}\right)^{12} - \left(\frac{d}{r}\right)^{6}\right] \tag{1}$$

where u_0 is the LJ energy, d is the LJ diameter and r is the distance between two interacting beads. Both u_0 and d were taken as unity.

The beads are bonded via a quartic bond potential (see (2))

$$U_q(r) = \begin{cases} k(y-b_1)(y-b_2)y^2 + U_0, & r < r_c, \\ U_0, & r > r_c \end{cases} \tag{2}$$

where $y = r - \Delta r$ that shifts the quartic center from the origin and the parameters as adopted directly from the study by Stevens et al. (Stevens 2001) are $k = 1434.3u_0/d^4$, $b_1 = -0.759d$, $b_2 = 0.0$, $\Delta r = r_c = 1.5d$ and $U_0 = 67.223u_0$. The bond potential is smoothly cutoff at r_c. At distances larger than r_c the bond potential is turned off that leaves only LJ term remaining. The bond breakage is irreversible. The bond potential parameters result in maximum bonding force of $156.7u_0/d$ compared to maximum LJ force of $2.4u_0/d$.

Coulombic interactions for pairs of ionic beads were computed with a cutoff of also $2.5d$(for the direct sum)

$$U_{\text{Coul}}(r) = k_B T \frac{l_B q_i q_j}{r} \tag{3}$$

where q_i is the charge on bead i, k_B is the Boltzmann constant, T is temperature, ε is dielectric constant and l_B is the Bjerrum length. l_B is defined as the separation distance at which the electrostatic interaction between two interacting elementary charges, e, in a dielectric medium with dielectric constant ε is equivalent to the thermal energy

$$l_B = \frac{e^2}{\varepsilon k_B T} \tag{4}$$

l_B was set to $50d$. With this value of l_B, the ratio of the maximum quartic bonding force to the ionic interaction force becomes about 4. Specifically, at $r = 1.12d$ the ionic force is $39.1u_0/d$ versus $156.7u_0/d$ (i.e. ratio of 4.0). This ratio is simply an estimate value that relates the strength of a typical covalent bond to an ionic bond.

The MD simulations were performed using LAMMPS (Large-scale Atomic/Molecular Massively Parallel Simulator) (Plimpton 1995). The equations of motion were integrated using the Verlet algorithm (Verlet 1967) with a time step of 0.05τ, where τ is the LJ time unit. The long-range Coulombic interactions beyond the cutoff (reciprocal sum) were calculated using the particle-particle particle-mesh Ewald (PPPM) solver with a precision value of 1.0×10^{-3}. Both the temperature and pressure were controlled using Nosé-Hoover formalism with a damping constant of 0.1τ.

The initial simulation box consisted of small chains with two and three beads that were sandwiched between two rigid layers of beads. The chains with three beads contained one bead designated as the cross-linker bead for the subsequent cross-linking process. The layers were made of (111) plane of the face-centered cubic (FCC) lattice structure with lattice spacing of 1.2. They interact with all beads except themselves. The system consisted of a total number of 103,344 beads of *chain*, *cross-linker* and *layer* type, where the ratio of the number of two- and three-bead chains was determined by stoichiometry. The liquid mixture was first equilibrated in canonical ensemble (NVT) at 1.0 reduced temperature unit (T^*), followed by the density equilibration in NPT (isobaric-isothermal) ensemble. The pressure was imposed anisotropically in z-axis while no pressure scaling was employed in x and y directions.

The liquid mixture was dynamically cross-linked after the equilibration. Briefly, a varying distance criterion was used first to determine the candidate pairs (i.e. a bead and a *cross-linker* bead with a functionality of four) which then were sequentially cross-linked. The

selected separation distance ranged from $1.1d$ at the first step until $1.35d$ at the final cross-linking step. Each step consisted of: 1. the determination of pairs, 2. the creation of bonds, and 3. the equilibration of the system. The cross-linking (first to the beads in the layers and then in the bulk) was carried on for a total of 40 and 60 steps, respectively. The number of steps for the first cross-linking stage was adjusted to create adequate cross-linking density on the layers so that cohesive failure was promoted. The second cross-linking stage was continued until a sufficient degree of cross-linking was achieved in the bulk. Near the end of each cross-linking stage, only a few or no additional cross-linking occurred. As a result, about 60,000 cross-linking bonds were created with nearly 5,000 of them bonded to the beads in the rigid layers, leading to 98% degree of cross-linking. After equilibration of the network at $1.0T^*$, the harmonic bond potential used hitherto was replaced with the quartic potential. Subsequently, the system was slowly cooled down (at a rate of $1.4 \times 10^{-5}T^*$ per MD step) to $0.3T^*$, which is well below the estimated glass transition temperature.

Ionic bonds were incorporated into the fully cross-linked network subsequent to its equilibration. The bond between a pair of randomly selected consecutive beads was removed to create ionic bonds. In the case of an ionic network, these beads were assigned opposite charges to create ionic bonds while for a standard network they were left unchanged. Using this approach, we created a new network with the same network density (82%) as non-ionic one but with ionic bonds incorporated within. The fact that we used pairs of beads bonded to each other to create ionic pairs is actually expected to reflect a molecular arrangement close to an actual system. Namely, one would anticipate in the actual synthesis of a polymeric network that the monomers with opposite charges would be at close proximity as the cross-linking reactions take place. However, there could also be multiplets where more than a pair of charged particles assembles. Therefore, our approach in creating the ionic network from a network that had no ionic interactions during cross-linking would yield an ideal network where there are no ionic aggregates, only pairs.

Two modes of deformation (tensile and shear) were applied in a quasi-equilibrium fashion. In the tensile mode, the upper layer was displaced along the z-direction with a selected speed over an increment of $0.5d$. Subsequently, the simulation was run at the new position for the same number of simulation steps needed for the displacement. The data for the calculation of the stress-strain curves were collected at this stage. The effective deformation rate, therefore, is half of the selected displacement speed. The two selected speeds 0.5×10^{-1} and $0.5 \times 10^{-2}d/\tau$ resulted in strain rates of 0.6×10^{-3} and $0.6 \times 10^{-4}\ 1/\tau$, respectively. In the case of the shear deformation the upper layer was displaced in the x-direction.

3 Results

We begin our analyses with an inspection of the microstructure of the ionic network using a set of radial distribution functions ($g(r)$) shown in Fig. 1. $g(r)_{chain\text{-}chain}$ exhibits an initial sharp peak located at 0.95 and a broader peak at $1.07d$ corresponding to the bonded and the non-bonded interactions among the beads of the *chain* type, respectively. In other words, the quartic bond potential with the parameters used in this study shows a minimum in the potential energy at $0.93d$ that agrees with the position of the initial peak, while the energy minimum in the Lennard-Jones potential for the non-bonded interactions is at $1.12d$ in line with the second peak. The remainder of the $g(r)_{chain\text{-}chain}$ has shallower and dying out peaks that is reminiscent of liquids. $g(r)_{xlinker\text{-}xlinker}$ is very similar to $g(r)_{chain\text{-}chain}$ suggesting that the *cross-linker* beads are uniformly distributed in the network. However, the absence of a sharp peak near $0.93d$ signifies that cross-linkers are not bonded to one another. The

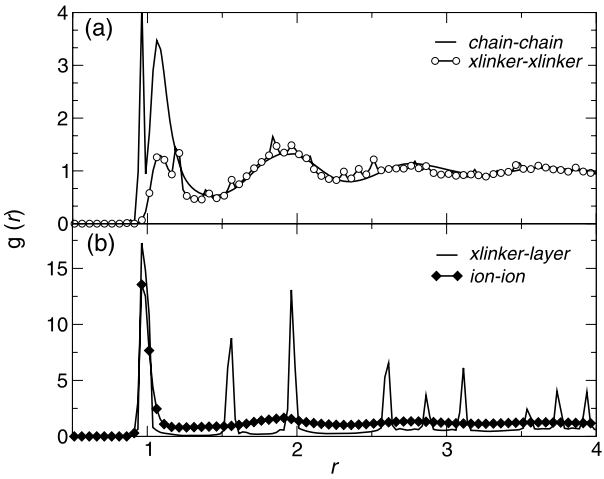

Fig. 1 Radial distribution functions of pairs of (**a**) *chain-chain* and *xlinker-xlinker* and (**b**) *ion-ion* and *layer-xlinker* type beads

sharp spike-like peaks in $g(r)_{xlinker\text{-}layer}$ indicate a layer by layer positioning of the *cross-linker* beads near the layers. The first peak is a result of *cross-linkers* directly bonded to the layers, while the second ($\sim 1.6d$) and third ($\sim 2.0d$) peaks are due to the *cross-linkers* that are separated from layers by one and two layers of beads, respectively. The intensity of these peaks diminishes rapidly with r. This type of arrangement shows that the network has a fairly ordered structure near the layers ($r < \sim 5d$) that becomes amorphous-like away from the layers. The relative positioning of the ionic pairs are represented by $g(r)_{ion\text{-}ion}$. There is a single and dominant peak at $0.97d$ pointing to the fact that they were created from pairs of beads which were initially bonded (i.e. pairs of a *cross-linker* and a *chain* type beads).

After this brief examination of the microstructure we will now investigate the material responses to the tensile deformation at low strains in order assess whether the current model follows the universal relationships between modulus, yield stress and temperature for cross-linked systems. The stress-strain curves for a fully cross-linked network (i.e. 98% degree of cross-linking) at temperatures ranging from 0.3 to $0.55T^*$ were plotted in Fig. 2(a). The Young's modulus (E), the yield stress (σ_y) and the strain at yield (ε_y) were extracted from these curves and are presented in Table 1. We first tested the Kambour's relationship (Kambour 1983),

$$\sigma_y = C(T_g - T) \tag{5}$$

which has been shown to be generally well fitted for thermosets (Cook et al. 1998; Tcharkhtchi et al. 1996). The linear relationship between σ_y and $T_g - T$ holds for our model as demonstrated in Fig. 2(b) with a fitted line to the data points.

Next, we investigate how the yield stress relates to the Young's modulus. It is well known that the ratio of σ_y/E is not constant, but a power law relationship proposed by Kitagawa (1977) was found to be valid for various thermosets (Cook et al. 1998; Yamini and Young 1980):

$$\frac{T_0\sigma_y}{T\sigma_{y,0}} = \left(\frac{T_0 E}{T E_0}\right)^n \tag{6}$$

where E_0 and $\sigma_{y,0}$ are the modulus and the yield stress at a reference temperature of T_0. The current model exhibits the same power law relationship between σ_y and E as presented in Fig. 2(c). However, the exponent n is calculated as 1.13 compared to the experimental

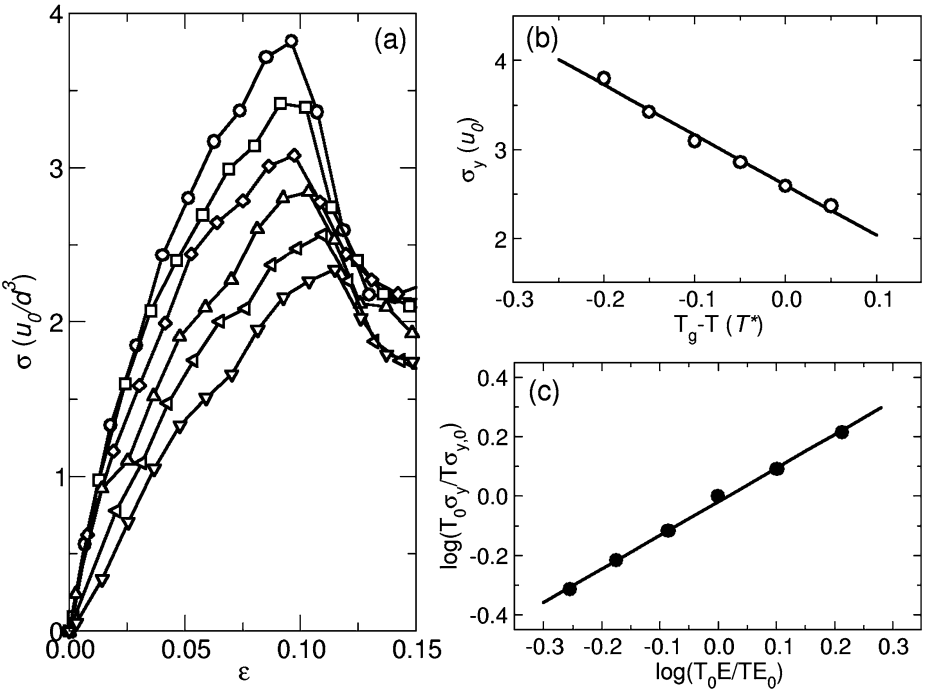

Fig. 2 (**a**) Stress-strain curves for a fully cross-linked network (98% degree of cross-linking) at varying temperatures ($T = 0.3$ (*circle*), 0.35 (*square*), 0.4 (*diamond*), 0.45 (*triangle up*), 0.5 (*triangle left*), 0.55 (*triangle down*) T^*). (**b**) Yield stress versus $T_g - T$ with a linear fit. T_g was taken as 0.5 T^* (Stevens 2001). (**c**) Yield stress and modulus data according to the equation proposed by (Kitagawa 1977). $T_0 = 0.4T^*$

Table 1 Young's Modulus, yield stress and yield strain for a fully cross-linked network (98% degree of cross-linking) at various temperatures

$T(T^*)$	$E(u_0/d^3)$	$\sigma_y(u_0/d^3)$	ε_y
0.3	50.0	3.8	0.090
0.35	43.8	3.4	0.095
0.4	40.6	3.1	0.096
0.45	34.9	2.9	0.098
0.5	30.8	2.6	0.100
0.55	27.0	2.4	0.110

result of 1.9. The difference might be resulting from the fact that the deformation rates in the simulations are several orders of magnitude higher than the experimental range. Since the strain rate appears to have a stronger effect on the yield stress than the modulus, the high deformation rates occurring in the simulations might be reducing the slope. Another reason could be the low chain stiffness in our model (i.e. the absence of bending and torsional potentials).

After comparing some mechanical properties of the simulations to empirical models at low strains for the fully cross-linked network, we turn our attention to mechanical responses in the tensile and the shear deformation for both the control and the ionic networks over the entire strain range. The stress-strain curves obtained after the tensile deformation are

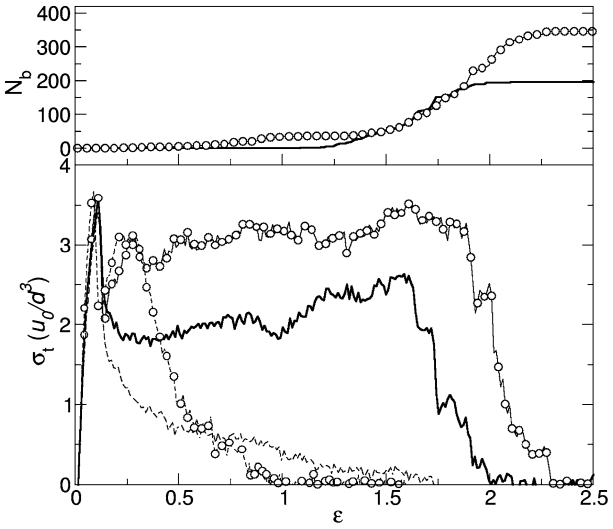

Fig. 3 Number of bonds (N_b) (upper panel) and stress (σ) versus strain (ε) upon the tensile deformation at strain rate of $0.6 \times 10^{-3}\ 1/\tau$ for the standard network (*line*) and the ionic network (*circles*). *Dashed lines* represent data for a network with higher degree of ionic content

shown in Fig. 3 (lower panel). There is a clear peak for both networks corresponding to the yield behavior at $\varepsilon = \sim 0.1$. The yield stress originates primarily from the LJ interactions. For this reason, the yield peak appears to be very distinct due to the fact that the networks have a lower degree of cross-linking than a fully cross-linked system such as in Fig. 2. The degree of cross-linking does not have direct influence on the yield stress; rather σ_y is affected indirectly due to the change in T_g (Pascault et al. 2002). However, the plateau is reduced significantly with lowering the degree of cross-linking. Therefore, σ_y becomes larger than the rest of the stress-strain curve since the degree of cross-linking was lowered to 82%. Note also that the equilibrium distance of the LJ potential is at $1.12d$, while the maximum force occurs at $1.25d$. Therefore, it takes a strain of about 0.1 to bring the network from the equilibrium LJ separation to a separation of the maximum resistance.

In the standard network, subsequent to the yield stress there is plateau region that lasts until about $\varepsilon = 1.0$. During this period the strands connecting two cross-linkers are being extended while bonds remain mostly intact as described by Stevens (2001). The bonds start breaking appreciably only after about $\varepsilon = 1.2$ (see upper panel in Fig. 3) and the network fails ultimately at about $\varepsilon = 2.0$. The ionic network exhibits a similar behavior to the standard network, but with some imperative differences. First, after the yield behavior the values of stress do not drop as extensively as the standard network. The stress-strain curve remains above that of the standard network indicating that the addition of ionic bonds improves the toughness (i.e. the area under this curve). Another key result is that the ionic network requires nearly twice as many bonds to be broken to fail compared to the standard network. We also observe that the ultimate failure does not occur abruptly due to the lower degree of cross-linking.

We ran a set of simulations for a network with 14% ions to observe how a larger ionic content and a lower degree of cross-linking affect stress-strain behavior. Following the same approach as in the Sect. 2, the resulting network had 66% degree of cross-linking. The standard network with 14% ionic content loses its strength (as compared to 7% ionic content) due to the fact that the network loses its structural integrity at the low level of cross-linking. In the case of the ionic network, the network provides additional strength (slightly higher than 7% ionic content) until $\varepsilon = \sim 0.3$ and then, stress drops rapidly to a level seen for the standard network.

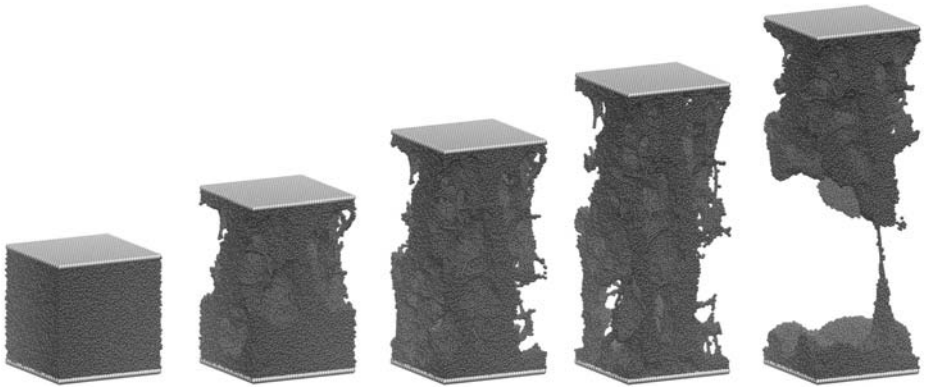

Fig. 4 Views of the network during deformation in the tensile mode at $\varepsilon = 0.0$, 0.5, 1.0, 1.5, and 2.0

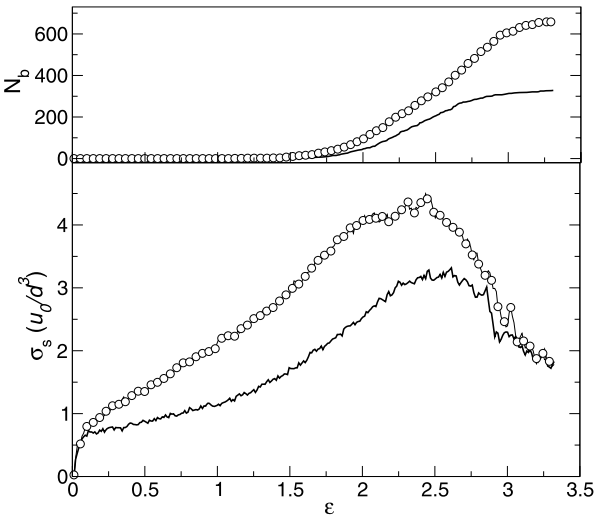

Fig. 5 Number of bonds (N_b) (*upper panel*) and stress (σ) versus strain (ε) upon the shear deformation at strain rate of $0.6 \times 10^{-3}\ 1/\tau$ for the standard network (*line*) and the ionic network (*circles*)

Snapshots of the network under tensile deformation at five consecutive strains are presented in Fig. 4 to aid visualizing the deformation in tensile mode. At $\varepsilon = 0.5$, there are voids formed in the network. They actually emerge as the strain passes through the yield point. Their formation does not require breaking of bonds since they are already present but are compacted. Moreover, their presence indicates that the cross-linking is not entirely homogenous: there are regions of highly dense cross-linking and those of lesser amount of cross-links. They basically act as defects that initiate cracks. At $\varepsilon = 1.0$, the voids grow further and the surrounding areas approach their limits of the stress they can carry without breaking of bonds. Later, at $\varepsilon = 1.5$, the stretching strands that bear the load become more visible. At this stage, there is a considerable degree of bond breaking and the network starts to break into two pieces. Finally, at $\varepsilon = 2.0$, the network has nearly failed with only a single strand holding the newly created interfaces.

The response to the deformation in the shear mode is presented in Fig. 5. The initial rapid rise of the stress and the subsequent slowing down at $\varepsilon = 0.1$ is due to the yield behavior. The magnitude of the yield stress for the standard network is $0.07u_0/d^3$ which is in

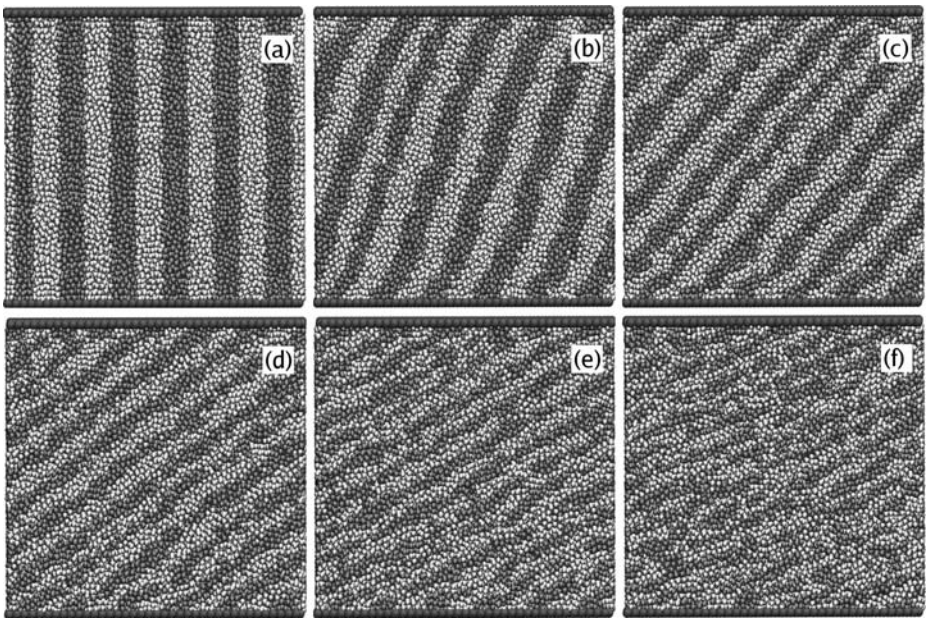

Fig. 6 Views of the network through x–z plane during the shear deformation at strain values of (**a**) 0.0, (**b**) 0.7, (**c**) 1.3, (**d**) 2.0, (**e**) 2.6, and (**f**) 3.3. The beads are colored in stripes to help visualize the shear deformation

agreement with $0.08u_0/d^3$ found in the earlier study (Stevens 2001). The yield stress in this deformation mode stems from the frictional resistance between two sliding surfaces interacting via LJ beads. After the yield point, stress continues to rise first, at a lower rate, and later ($\varepsilon > \sim 1.2$) at a higher rate until it reaches the maximum point (i.e. where the ultimate failure occurs). Note that the bond breaking continues even after the maximum point, because the failure results in a rough interface. This interface is smoothened while being sheared, thus bond breaking continues until two sufficiently smooth surfaces are attained. Subsequently, the shearing would constitute shearing of two flat surfaces interacting via LJ interactions similar to the case at the yield point. Therefore, if simulation was pursued further the stress would eventually level off at about the yield stress.

In the earlier studies (Stevens 2001; Tsige et al. 2004) the maximum point was followed by a sudden drop in stress. This drop is more gradual in our study because of the lower degree of cross-linking since densely cross-linked networks fail more abruptly. The comparison of the networks shows that the stress increases in the ionic network more rapidly than the standard network and maintains its elevated level until the point of the maximum stress. Similar to what was found in the deformation in the tensile mode, the incorporation of ionic pairs raises the shear stress thus generating a tougher network. However, after the maximum stress is reached both curves become nearly overlapping. We discuss this behavior in the following section.

The deformation the in the shear mode is illustrated in Fig. 6(a) through (f) using six snapshots taken at ascending strain values. At $\varepsilon = 0.7$, the stripes are stretched to a sigmoidal-like shape. As the network is stretched further at $\varepsilon = 1.3, 2.0$ and 2.6 they get straighter and thinner showing that the strands are extended at or beyond their limits before

breaking. Finally, at $\varepsilon = 3.3$, close observation reveals that the location of interfacial failure is near the middle of the lower half of Fig. 6(f).

4 Discussion

Our generic coarse-grained model for the networks reproduced the general features in a stress-strain curve such as the yield behavior, the leveling of the stress after the yield point, the subsequent strain hardening, and the failure. Additionally, we presented some agreements to the universal empirical models for thermosets (i.e. how σ_y changes with T and how it relates to E). Even though, the quantities we calculate are in the LJ units, we attempt to relate them to some empirical results. The issue is to relate the units of stress from the LJ units in our simulations to the real units in experiments. The unit stress, u_0/d^3, was estimated to be equivalent to 43 MPa by calculating the stress required to separate a model self-assembled monolayer (composed of beads with the same interaction parameters as in this work) from a rigid surface to its experimental equivalence (Stevens 2001). We use this approximate value in order to put the predictions of this model into experimental perspective for a fully cross-linked network with no ions.

The estimated values for σ_y and E from the simulations were compared to the experimental data (Fig. 7). σ_y has a linear dependency on $T_g - T$ for both the experimental and the simulation data, as mentioned previously. However, the model predicts a lower slope than the experiments and the model fails to predict that σ_y should vanish as T approaches to T_g, as suggested by the empirical data. Nonetheless, the model appears to be providing a good quantitative agreement (with the assumption that $u_0/d^3 = 43$ MPa) at about $T_g - T = 125$ K (i.e. at $T = 0.3T^*$ in LJ units). Coincidentally, this is the temperature when the simulations of the tensile and the shear deformations were performed. The estimates of the modulus

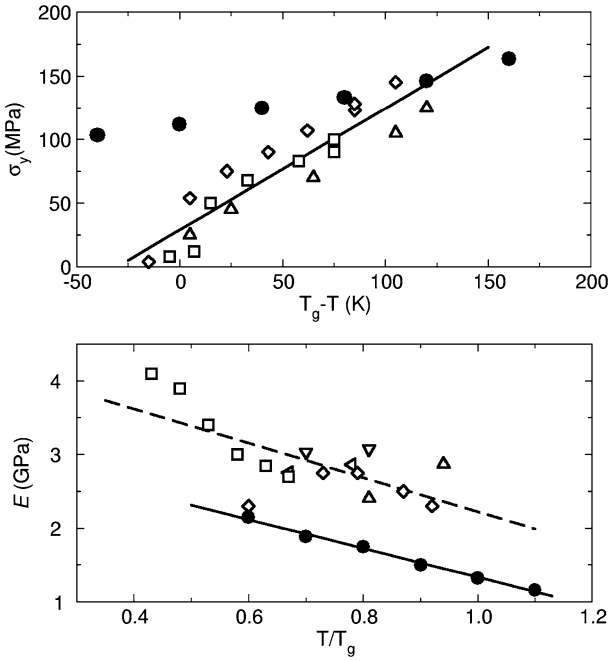

Fig. 7 (**a**) Yield stress versus $T_g - T$. Estimated values for σ_y from the simulations (*closed circle*) were compared with experiments for different epoxy thermosets: DGEBA/DDM (*diamond*), DGEBA/BA (*square*), and DGEBA/DAO (*triangles*) (Cook et al. 1998). T_g for the model network of 0.5 T^* was assumed to be equivalent to 400 K in real units. (**b**) The Young's modulus versus T/T_g. Estimated values for E from the simulations (*closed circle*) were compared with experiments for different epoxy thermosets: RTM6 (*square*), Araldite-F (*diamond*) (Deng et al. 2007), DGEBA (*triangle up*), TGAP (*triangle left*), and TGDDM (*triangle down*) (Becker et al. 2003). The slopes for the fits are 2.0 and 2.3 for the simulation and the experimental data, respectively

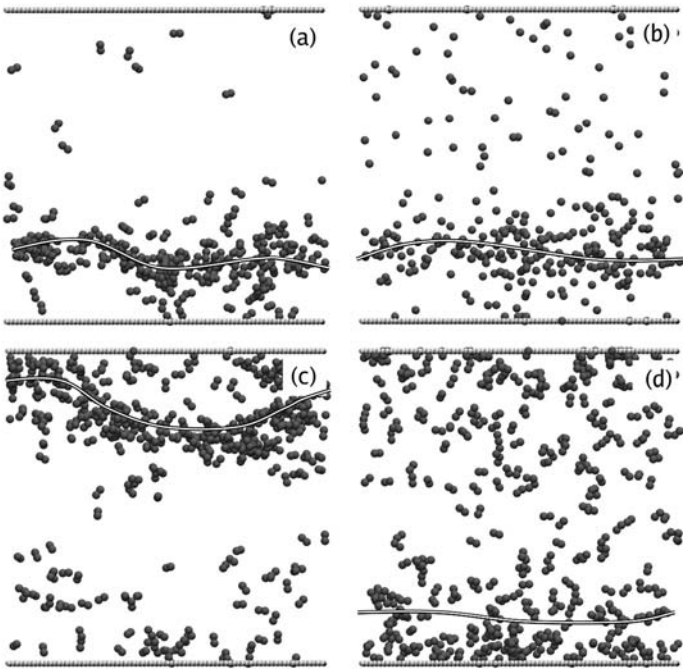

Fig. 8 Views (through x–z plane) of pairs of beads forming bonds that eventually brake after applying deformation. The upper half shows views for the control network after the deformation in (**a**) tensile and (**b**) shear mode. Similarly, the lower half shows views for the ionic network after the deformation in (**c**) tensile and (**d**) shear mode. The lines highlight approximate locations of the ultimate interfacial failure

from the simulations show a quite similar dependency on T/T_g and they are about 1 GPa lower compared to the experimental data. Note that our model does not take into account the chemical structure of the repeating units in epoxy resins and that the experimental control parameters such as the deformation rate and the sample size are several orders of magnitude higher than the simulations. Therefore, this minimal model shows a remarkable agreement with experiments considering the simplicity of the model and the differences in such experimental parameters.

The number of bonds that broke after deformation is an important quantity as it relates to the failure mechanism. We found consistently in both the tensile and shear modes that the ionic network requires a larger number of bonds to be broken before the ultimate failure occurs. In order to understand the origins of this behavior, we first determined the positions of the failing bonds. These bonds, as identified in Fig. 8, indicate the location of the interfacial failure. For example, the clustering of these broken bonds in the lower portion of the Fig. 8(a) points to the location of failure as confirmed by Fig. 4 for the deformation of the standard network in the tensile mode. Figure 8(c) shows that, in the case of the ionic network, these bonds are present not only in the location of the failure but also in the surrounding area by a larger quantity than the control network (Fig. 8(a)). This result is even clearer in shear mode (Fig. 8(b) vs. (d)).

We infer from these observations that the integration of ionic pairs brings about a network that can distribute the stress more uniformly, which in turn results in improved mechanical properties. In order to gain insight into how the stress is distributed more uniformly we looked at the growth of voids that form with tensile deformation. It is an important phe-

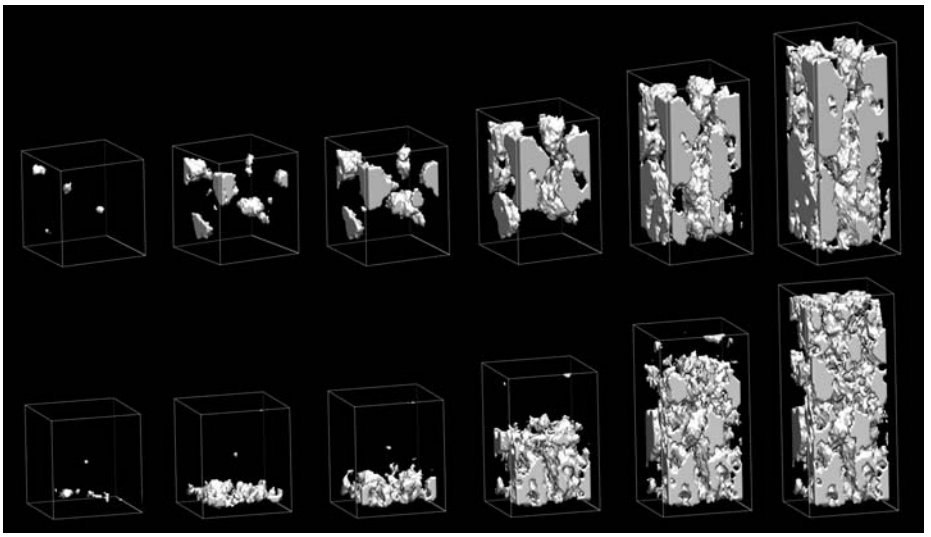

Fig. 9 Snapshots of the voids as they develop during the tensile deformation in the standard (*upper panel*) and the ionic (*lower panel*) networks. Strains at which snapshots were generated are (*from left to right*): 0.1, 0.15, 0.25, 0.5, 1.0 and 1.5

nomenon because the strands surrounding voids are where the stresses concentrate. The snapshots of voids are shown in Fig. 9 at varying strains. At the yield point ($\varepsilon = 0.1$), the voids are visible in their early form. They appear to be more randomly distributed initially in the standard than the ionic network, while at strains $\varepsilon > 1.0$ they are equally randomly distributed. The variation in their distribution is not expected to affect the mechanical properties significantly, because the difference in randomness is seen only until bond breaking starts. However, it is notable to observe that the sizes of the voids are smaller in the ionic network compared to the standard network at any strain. The smaller void sizes the larger the area separating the material from the empty space. This means that the stress concentration is not as severe and the load can be more uniformly distributed throughout the network. This observation supports the analysis of the distribution of broken bonds in showing how the mechanical properties are improved.

We had observed earlier that the shear stress is enhanced up to the point of the interfacial failure (Fig. 5). After this point, stresses became indistinguishable between the two types of networks. Unlike this observation, when a lower deformation rate (by an order of magnitude) is applied (see Fig. 10), the ionic network continues to bear a higher load even after the point of the maximum stress. Knowing that the two experiments differ only by the deformation rate and that the networks differ only by the presence of ionic pairs, this result indicates that it is a consequence of the rate dependence of ionic pairs. A plausible explanation is that the ionic pairs that deform as a result of shearing are able to re-form only when the system is deformed with a low strain rate so that the strands have enough time to relax. We infer also that this time dependency refers to the presence of a self-healing mechanism that restores the some of the strength of the network.

The ionic interactions were introduced to the network in randomly distributed pairs as explained above. This approach has been followed in order, besides its practicality, to evaluate the concept of ionic interactions when they are incorporated in the network ideally: each charged particle interacting with its counterpart. However, if the ionic interactions

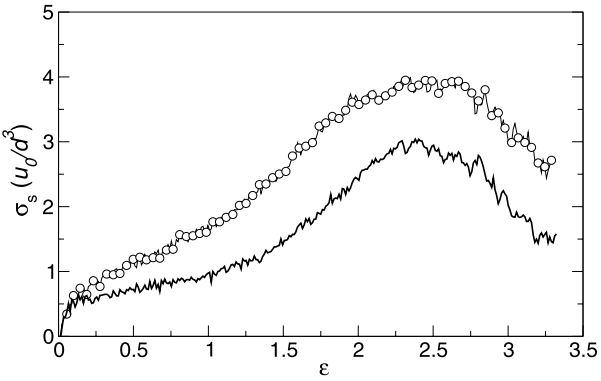

Fig. 10 Stress (σ) versus strain (ε) upon the shear deformation at strain rate of $0.6 \times 10^{-4}\ 1/\tau$ for the standard network (*line*) and the ionic network (*circles*)

were present during the cross-linking stage, the resulting network might have had a different structure. While one would expect to observe oppositely charged particles interacting thus being in close proximity, they could be in the form of small clusters rather than pairs. Therefore, the results of this work should be interpreted with this fact in consideration.

5 Concluding remarks

We presented results for a coarse-grained model of cross-linked networks with and without ionic bonds incorporated. The MD simulations of the deformation of the networks in tensile and shear mode showed that the model has captured the fundamental mechanical features of thermosets such as the yield behavior, the leveling of the stress after the yield point, the subsequent strain hardening, and the failure. Moreover, we presented some agreements to the universal empirical models for thermosets at both qualitative and quantitative level.

One is bound by the length scale that can be practically modeled, as an inherent limitation of molecular level simulations. This constraint reflected itself for the current system in two ways. First, how the stress is transferred from the solid layers to the network should be a function of the distance between the upper and lower layers. The interfacial failures that occur in the vicinity of the layers, rather than in the middle section in all four cases may be a consequence of the stress build up in this region. Secondly, the network can be only as heterogeneous as the system size. In fact, the main reason why the system fails only after very high strains ($\varepsilon > 2$) is that the crack initiation can occur only after strands are extended significantly. In a real material there would be *a heterogeneous cross-linking* (i.e. broad distribution of degree of freedom of strands to stretch). When the deformation is applied, the strands with a low degree of freedom to stretch will be stressed the most and break first. These regions where such constrained strands concentrate will act as defects that initiate cracks before the rest could collectively stretch. For this reason, the smaller the samples size the lower the probability of having defects in the material that results in higher stress at break (Pascault et al. 2002). From this point of view, the current model appears to represent an ideal network compared to a real one. Another interpretation is that the model is capturing the deformation behavior at or near the crack tip as suggested previously (Stevens 2001; Tsige et al. 2004; Tsige and Stevens 2004).

The primary outcome of this work is the finding that the integration of ionic pairs in an ideal manner elevated the level of stress that the network can withstand over a wide range of strain values in both the tensile and shear modes. This implies that the ionic pairs

create a stronger and tougher network compared to the control network. We identified two plausible mechanisms through which the ionic pairs became effective. They enable a more uniform distribution of the stress through the network and they are able to reform after being displaced by deformation at low strain rates.

In future work, we plan to investigate the effects of the cross-link density, content of ionic pairs and the interplay between them. The formation of the network in the presence of ionic reactants will also be carried out to determine whether it leads to a different network structure.

Acknowledgements The authors thank Maj. Jennifer Gresham of the Air Force Office of Scientific Research for sponsorship of this work under the AFRL "Smart Surfaces" program. Authors are thankful to Mesfin Tsige for his helpful suggestions.

References

Balazs, A.C.: Modeling self-healing materials. Mater. Today **10**, 18–23 (2007). doi:10.1016/S1369-7021(07)70205-5

Becker, O., Cheng, Y.-B., Varley, R.J., Simon, G.P.: Layered silicate nanocomposites based on various high-functionality epoxy resins: the influence of cure temperature on morphology, mechanical properties, and free volume. Macromolecules **36**, 1616–1625 (2003). doi:10.1021/ma0213448

Cook, W.D., Mayr, A.E., Edward, G.H.: Yielding behaviour in model epoxy thermosets, II: temperature dependence. Polymer (Guildf.) **39**, 3725–3753 (1998). doi:10.1016/S0032-3861(97)10335-4

Deng, S., Hou, M., Ye, L.: Temperature-dependent elastic moduli of epoxies measured by DMA and their correlations to mechanical testing data. Polym. Test. **26**, 803–813 (2007). doi:10.1016/j.polymertesting.2007.05.003

Din, X.D., Michaelides, E.E.: Transport processes of water and protons through micropores. AIChE J. **44**, 35–47 (1998). doi:10.1002/aic.690440106

Eisenberg, A., Hird, B., Moore, R.B.: A new multiplet-cluster model for the morphology of random ionomers. Macromolecules **23**, 4098–4107 (1990). doi:10.1021/ma00220a012

Elliott, J.A., Hanna, S., Cooley, G.E.: Atomistic simulation and molecular dynamics of model systems for perfluorinated ionomer membranes. Phys. Chem. Chem. Phys. **1**, 4855–4863 (1999). doi:10.1039/a905267d

Heine, D.R., Grest, G.S., Lorenz, C.D., Tsige, M., Stevens, M.J.: Atomistic simulations of end-linked poly(dimethylsiloxane) networks: structure and relaxation. Macromolecules **37**, 3857–3864 (2004). doi:10.1021/ma035760j

Kambour, R.P.: Correlations of the dry crazing resistance of glassy polymers with other physical properties. Polym. Commun. (Guildf.) **24**, 292–296 (1983)

Kessler, M.R.: Self-healing: a new paradigm in materials design. Proc. Inst. Mech. Eng. G **221**, 479–495 (2007). doi:10.1243/09544100JAERO172

Kitagawa, M.: Power law relationship between yield stress and shear modulus for glassy polymers. J. Polym. Sci. Polym. Phys. Ed. **15**, 1601–1611 (1977). doi:10.1002/pol.1977.180150907

Pascault, J.-P., Sautereau, H., Verdu, J., Williams, R.J.J.: Thermoseting Polymers. Marcel Dekker, New York (2002)

Plimpton, S.: Fast parallel algorithms for short-range molecular dynamics. J. Comput. Phys. **117**, 1–19 (1995). doi:10.1006/jcph.1995.1039

Stevens, M.J.: Interfacial fracture between highly cross-linked polymer networks and a solid surface: effect of interfacial bond density. Macromolecules **34**, 2710–2718 (2001). doi:10.1021/ma000553u

Tadano, K., Hirasawa, E., Yamamoto, H., Yano, S.: Order-disorder transition of ionic clusters in ionomers. Macromolecules **22**, 226–233 (1989). doi:10.1021/ma00191a043

Tcharkhtchi, A., Faivre, S., Roy, L.E., Trotignon, J.P., Verdu, J.: Mechanical properties of thermosets, part I: tensile properties of an anhydride cured epoxy. J. Mater. Sci. **31**, 2687–2692 (1996). doi:10.1007/BF00687301

Tsige, M., Stevens, M.J.: Effect of cross-linker functionality on the adhesion of highly cross-linked polymer networks: a molecular dynamics study of epoxies. Macromolecules **37**, 630–637 (2004). doi:10.1021/ma034970t

Tsige, M., Lorenz, C.D., Stevens, M.J.: Role of network connectivity on the mechanical properties of highly cross-linked polymers. Macromolecules **37**, 8466–8472 (2004). doi:10.1021/ma049074b

Verlet, L.: Computer “experiments” on classical fluids, I: thermodynamical properties of Lennard-Jones molecules. Phys. Rev. **159**, 98–103 (1967). doi:10.1103/PhysRev.159.98

Vishnyakov, A., Neimark, A.V.: Molecular simulation study of nafion membrane solvation in water and methanol. J. Phys. Chem. B **104**, 4471–4478 (2000). doi:10.1021/jp993625w

Yamini, S., Young, R.J.: The mechanical properties of epoxy resins. J. Mater. Sci. **15**, 1823–1832 (1980). doi:10.1007/BF00550603

Yarovsky, I., Evans, E.: Computer simulation of structure and properties of crosslinked polymers: application to epoxy resins. Polymer (Guildf.) **43**, 963–969 (2002). doi:10.1016/S0032-3861(01)00634-6